JOURNAL OF THE GEOTECHNICAL ENGINEERING DIVISION

LONGITUDINAL VIBRATIONS OF EMBANKMENT DAMS

By George Gazetas,[1] A. M. ASCE

INTRODUCTION

The types of serious damage that are most frequently observed in embankment dams after strong earthquakes can be grouped into the following four categories in order of increasing frequency of occurrence (9):

1. Longitudinal cracks that develop especially near the crest due either to tensile stresses caused by the lateral vibrations of the dam or to differential settlements caused by different degrees of dynamic compaction of various dam zones (core, shell) or foundation soils.
2. Slides of soil masses from the upstream or downstream slope of the dam triggered by lateral vibrations that induce along sliding surfaces shear stresses that exceed, on the average, the shear strength of the soil.
3. Transverse cracks that develop usually near the abutment-dam interfaces either due to tensile stresses created by longitudinal vibrations of the dam or due to differential settlements of various sections of the dam in the longitudinal direction.
4. Large displacements or bearing capacity failure due to liquefaction of saturated cohesionless soils in the dam or the foundation.

Transverse cracking due to longitudinal vibrations is neither as serious damage as are the large permanent deformations caused by liquefaction or sliding, nor as frequent a phenomenon as is the development of longitudinal cracks. This perhaps explains why so little attention has been directed towards understanding the behavior of earth dams when excited in a direction parallel to their axis. In contrast, extensive experimental and theoretical research has been related to lateral vibrations of earth dams or embankments (1,2,3,4,5,7,9).

[1]Asst. Prof. of Civ. Engrg., Case Western Reserve Univ., Cleveland, Ohio 44106.

Note.—Discussion open until June 1, 1981. To extend the closing date one month, a written request must be filed with the Manager of Technical and Professional Publications, ASCE. Manuscript was submitted for review for possible publication on December 18, 1979. This paper is part of the Journal of the Geotechnical Engineering Division, Proceedings of the American Society of Civil Engineers, © ASCE, Vol. 107, No. GT1, January, 1981. ISSN 0093-6405/81/0001-0021/$01.00.

However, transverse cracks can be potentially very dangerous since they can induce uncontrolled seepage through the dam and thereby create piping failure(s). Such cracks are highly probable to occur especially at the contact surfaces of an embankment dam with its steep-sloping rock abutments, because of the different dynamic response of the two media, and because no tensile forces can develop between them. The 1/16-in. wide (1.6 mm) lateral crack which occurred at the east abutment of the Santa Felicia Dam during the San Fernando Earthquake of February 9, 1971, as reported by Abdel-Ghaffar and Scott (1) seems to have been of this nature.

The contact areas between soil and outlet works such as side spillways, sluiceways, and buried pipes are also vulnerable to tensile longitudinal stresses. Furthermore, cracking and ruptures of pipes observed after earthquakes have been attributed to the incompatibility of their displacements with the larger longitudinal deformations of the surrounding soil (9). Since many of these damages occur within the body of the dam and can easily remain undetected they may cause additional problems in the post-earthquake life of the structure. Consequently, experimental and theoretical research on the behavior of embankment dams during earthquake-induced longitudinal vibrations is urgently needed to develop methods of analysis, establish performance criteria, improve current design procedures, and invent rehabilitation techniques to ensure the safety of new or existing earth and rockfill dams during and after earthquakes.

As a first step in the aforementioned direction, this paper presents a theoretical analysis of free and forced vibrations of embankment dams. The method accounts for both dilatational and shear deformations and models the dam as a linear homogeneous triangular prism, bounded in the longitudinal direction by two vertical planes (rectangular canyon). Numerical results are presented for the natural frequencies, modal displacement, modal strain shapes, and modal participation factors. It is shown that in relatively long dams shear deformations are more important than axial deformations, whereas the reverse is true with dams that are built in narrow canyons. Two case studies are then presented in order to evaluate the ability of the presented theory to explain with reasonable accuracy observed field behavior. Natural frequencies, participation factors, and mode shapes computed with the theory for the Santa Felicia Dam in California and the Kisenyama Dam in Japan are examined in the light of observed predominant frequencies and peak response amplitudes of motions recorded during actual earthquakes (1,9). Finally the method is extended to approximately account for a realistic variation of shear modulus at various depths below the crest of the dam.

Analysis for Homogeneous Dam in Rectangular Canyon

Free Vibrations.—Let x, y, and z be the orthogonal coordinates of any point in a symmetrical earth dam built in a rectangular canyon, as shown in Fig. 1(*a*). To derive the governing equation of motion the simplifying assumption is made that normal and shear stresses, σ_x and τ_{zx}, are independent of y and, therefore, that σ_x and τ_{zx} are uniformly distributed over infinitesimal areas $b_y \cdot dz$ and $b_y \cdot dx$ respectively, as shown in Fig. 1(*b*). This assumption is reminiscent of the hypothesis of uniform shear stresses τ_{zy} over areas $b_y \cdot dx$ that is the basis of the shear-beam theory for lateral vibrations (3,4,7,9). It seems, however,

that the present hypothesis is more realistic since it does not violate the physical requirement of zero shear and normal stresses on the upstream and downstream faces of the dam, in contrast with the shear-beam assumption.

As a direct consequence of the foregoing assumption, the horizontal displacements are considered independent of y, i.e., $u = u(x, z; t)$. The differential

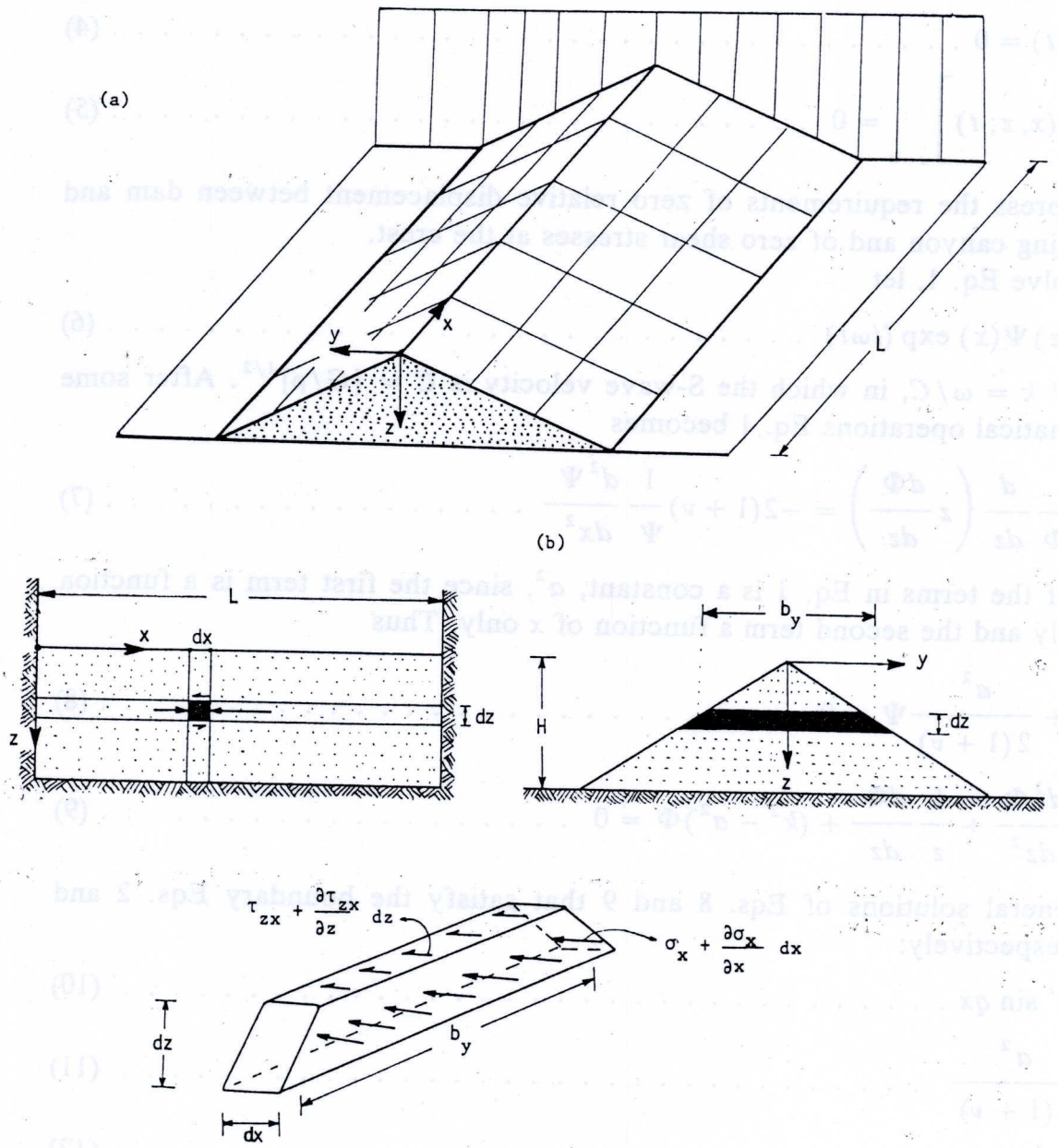

FIG. 1.—(*a*) Dam Geometry in Perspective; and (*b*) Longitudinal and Cross Section of Dam: Stresses Acting on Infinitesimal Body

equation that governs the spatial and temporal variation of u is subsequently derived from the dynamic equilibrium of an infinitesimal body of volume $b_y \cdot dx \cdot dz$ [Fig. 1(*b*)]:

$$\rho \ddot{u} - \frac{1}{z}\frac{\partial}{\partial z}\left(G z \frac{\partial u}{\partial z}\right) - \frac{\partial}{\partial x}\left(E \frac{\partial u}{\partial x}\right) = 0 \quad \ldots\ldots\ldots\ldots\ldots\ldots\ldots\ldots (1)$$

in which G and E = the shear and Young's moduli of the soil, herein taken as constants throughout the dam. The three terms in Eq. 1 express respectively the inertia, shear, and axial forces acting on the said infinitesimal body.

Solutions of Eq. 1 would be physically acceptable only if they satisfy the boundary conditions:

$$u(o, z; t) = 0 \quad \ldots\ldots (2)$$

$$u(L, z; t) = 0 \quad \ldots\ldots (3)$$

$$u(x, H; t) = 0 \quad \ldots\ldots (4)$$

$$G \frac{\partial}{\partial z} u(x, z; t) \Big]_{z=0} = 0 \quad \ldots\ldots (5)$$

that express the requirements of zero relative displacement between dam and supporting canyon and of zero shear stresses at the crest.

To solve Eq. 1, let

$$u = \Phi(z)\Psi(x) \exp(i\omega t) \quad \ldots\ldots (6)$$

and call $k = \omega / C$, in which the S-wave velocity is $C = [G/\rho]^{1/2}$. After some mathematical operations Eq. 1 becomes

$$k^2 + \frac{1}{z\Phi} \frac{d}{dz} \left(z \frac{d\Phi}{dz} \right) = -2(1 + \nu) \frac{1}{\Psi} \frac{d^2\Psi}{dx^2} \quad \ldots\ldots (7)$$

Each of the terms in Eq. 1 is a constant, a^2, since the first term is a function of z only and the second term a function of x only. Thus

$$\frac{d^2\Psi}{dx^2} + \frac{a^2}{2(1 + \nu)} \Psi = 0 \quad \ldots\ldots (8)$$

$$\text{and} \quad \frac{d^2\Phi}{dz^2} + \frac{1}{z} \frac{d\Phi}{dz} + (k^2 - a^2)\Phi = 0 \quad \ldots\ldots (9)$$

The general solutions of Eqs. 8 and 9 that satisfy the boundary Eqs. 2 and 5 are respectively:

$$\Psi = B' \sin qx \quad \ldots\ldots (10)$$

$$q^2 = \frac{a^2}{2(1 + \nu)} \quad \ldots\ldots (11)$$

$$\text{and} \quad \Phi = B'' J_0(bz) \quad \ldots\ldots (12)$$

$$b^2 = k^2 - a^2 \quad \ldots\ldots (13)$$

in which B', B'' = integration constants; and $J_0(\cdot)$ = Bessel Function of the first kind and zero order.

Enforcement of the other two boundary conditions (Eq. 3 and Eq. 4) leads to

$$a_r = \frac{[2(1 + \nu)]^{1/2}}{L} r\pi; \quad r = 1, 2, 3, \ldots \quad \ldots\ldots (14)$$

$$b_n = \frac{S_n}{H}; \quad n = 1, 2, 3, \ldots \quad \ldots\ldots (15)$$

in which S_n = the roots of $J_0(S) = 0$, e.g., $S_1 = 2.4048$, $S_2 = 8.6530$, etc. The natural frequencies for longitudinal vibrations are then obtained by combining Eqs. 13, 14, and 15:

$$\omega_{nr} = \frac{C}{H}\left[S_n^2 + 2(1+\nu)\,\pi^2\left(\frac{H}{L}\right)^2 r^2\right]^{1/2} \quad \ldots\ldots\ldots\ldots\ldots\ldots\ldots\ldots \quad (16)$$

while the displacement shapes, normalized to a unit peak amplitude, are given by

$$U_{nr} = J_0\left(S_n \frac{z}{H}\right) \sin\left(r\pi \frac{x}{L}\right) \quad \ldots\ldots\ldots\ldots\ldots\ldots\ldots\ldots\ldots\ldots \quad (17a)$$

$$u_{nr} = U_{nr} \exp(i\omega_{nr} t); \quad n, r = 1, 2, 3, \ldots \quad \ldots\ldots\ldots\ldots\ldots\ldots\ldots \quad (17b)$$

and the normal and shear strains by

$$\epsilon_{x,nr} = \frac{\partial u_{nr}}{\partial x} = \frac{r\pi}{L} J_0\left(S_n \frac{z}{H}\right) \cos\left(r\pi \frac{x}{L}\right) \exp(i\omega_{nr} t) \quad \ldots\ldots\ldots\ldots \quad (18)$$

$$\gamma_{zx,nr} = \frac{\partial u_{nr}}{\partial z} = \frac{S_n}{H} J_1\left(S_n \frac{z}{H}\right) \sin\left(r\pi \frac{x}{L}\right) \exp(i\omega_{nr} t) \quad \ldots\ldots\ldots\ldots \quad (19)$$

Earthquake-Induced Vibrations.—During earthquake shaking that consists exclusively of vertically propagating S-waves polarized in the x direction, the longitudinal motion of the dam relative to the surrounding canyon is described by

$$\rho\ddot{u} - \frac{1}{z}\frac{\partial}{\partial z}\left(Gz\frac{\partial u}{\partial z}\right) - \frac{\partial}{\partial x}\left(E\frac{\partial u}{\partial x}\right) = \rho\,\ddot{u}_{gx} \quad \ldots\ldots\ldots\ldots\ldots\ldots \quad (20)$$

in which $\ddot{u}_{gx}(t)$ = the ground acceleration (in the x direction), and by Eqs. 2, 3, 4, and 5 (boundary conditions). The solution is obtained by modal superposition (8):

$$u(x, z; t) = \sum_{n=1,2}^{\infty} \sum_{r=1,2}^{\infty} \Gamma_{nr}\, U_{nr}(x, z)\, D_{nr}(t) \quad \ldots\ldots\ldots\ldots\ldots\ldots\ldots\ldots \quad (21)$$

whereby, the modal participation factor Γ_{nr} of the n, r mode is

$$\Gamma_{nr} = \frac{\int_0^H \int_0^L U_{nr} \cdot y \cdot dx \cdot dz}{\int_0^H \int_0^L U_{nr}^2 \cdot y \cdot dx \cdot dz} = \frac{8}{\pi\, r\, S_n\, J_1(S_n)} \quad \ldots\ldots\ldots\ldots\ldots\ldots \quad (22)$$

while the modal response $D_{nr}(t)$ is obtained from the Duhamel integral:

$$D_{nr}(t) = \frac{1}{\omega^*_{nr}} \int_0^t \ddot{u}_{gx}(t) \exp\left[-\beta_{nr}\omega_{nr}(t-p)\right] \sin\left[\omega^*_{nr}(t-p)\right] dp \quad \ldots\ldots \quad (23a)$$

$$\omega^*_{nr} = \omega_{nr}(1 - \beta^2_{nr})^{1/2} \quad \ldots\ldots\ldots\ldots\ldots\ldots\ldots\ldots\ldots\ldots\ldots \quad (23b)$$

in which β_{nr} = damping ratio in the n, r mode.

Numerical Results

Fig. 2 demonstrates the relationship between natural frequencies, ω_{nr}, of a homogeneous dam in a rectangular canyon and the key geometric parameter, i.e., the length-to-height ratio, L/H. Specifically, Fig. 2(a) shows the decrease of the fundamental frequency-ratio, $\omega_{11} H/C$, as L/H increases, for two values

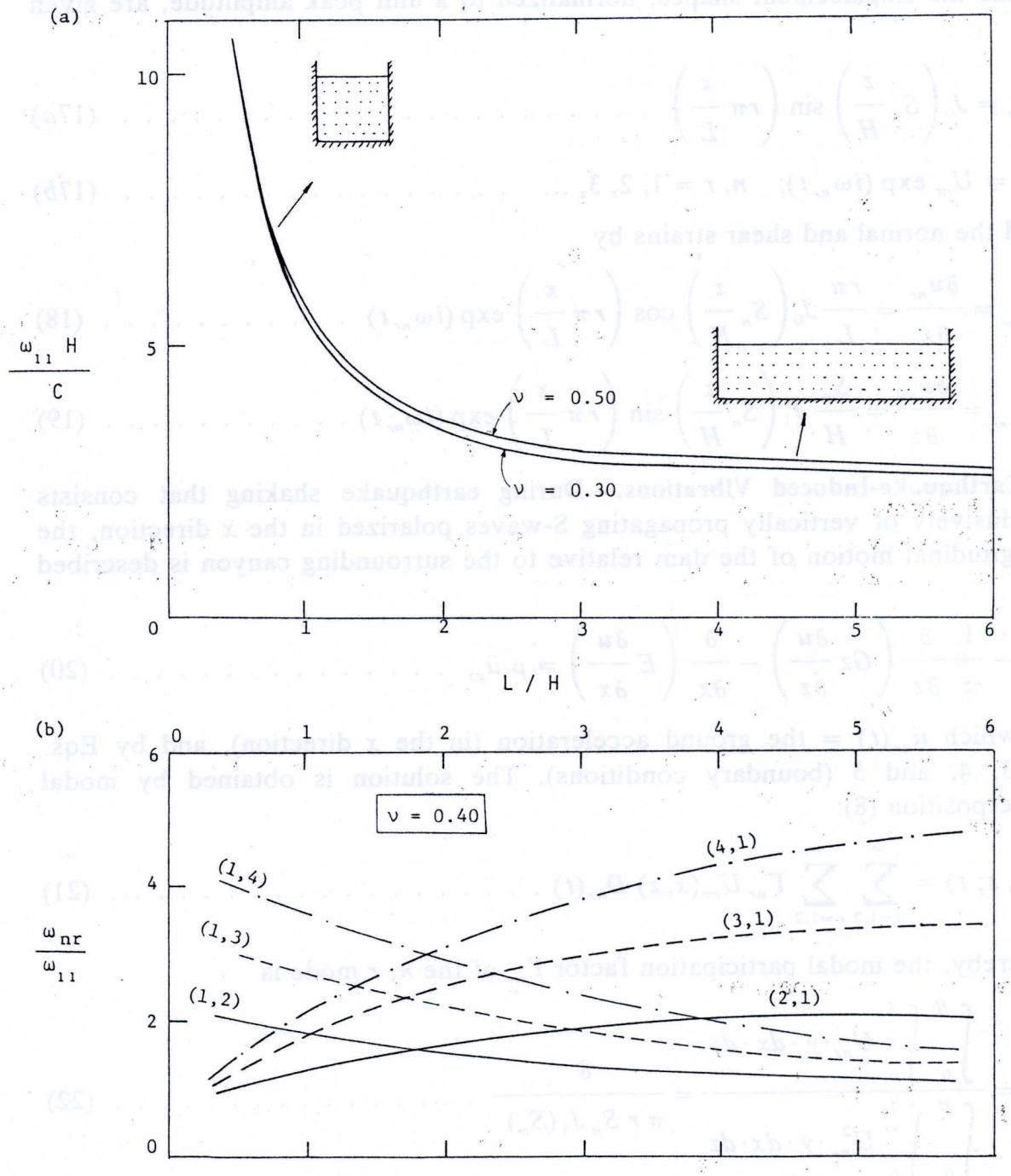

FIG. 2.—Dependence of Natural Frequencies on Length-to-Height Ratio

of Poisson's ratio, $\nu = 0.30$ and $\nu = 0.5$. One can clearly distinguish two regions in the frequency-ratio spectrum, corresponding to "narrow" or "wide" canyons, respectively. When L/H is less than about 1.5 ("narrow" canyon) $\omega_{11} H/C$ is inversely proportional to L/H, whereas when L/H is greater than about 2 ("wide" canyon) $\omega_{11} H/C$ is practically independent of L/H. The following expressions can be derived from Fig. 2(a) for the fundamental period in

longitudinal vibrations of "narrow" or "long" dams:

$$T_{11} \simeq 1.20 \frac{L}{C} \quad \text{for} \quad \frac{L}{C} \leq 1.5 \qquad (24a)$$

and $$T_{11} \simeq 2.80 \frac{H}{C} \quad \text{for} \quad \frac{L}{H} \geq 2 \qquad (24b)$$

Eq. 24*a* states that, for a narrow dam, T_{11} is independent of the height, H, and is only a function of the length, L, and the S-wave velocity, C. This result can be compared with the fundamental period in axial vibrations of a uniform rod fixed at both ends and having a Poisson's ratio $\nu = 0.40$:

$$T_1 \simeq 1.19 \frac{L}{C} \qquad (25a)$$

The similarity of Eq. 24*a* and Eq. 25*a* suggests that axial deformations are more significant than shear deformations in narrow dams.

The reverse appears to be true in long dams; T_{11} depends only on the height, H, of the dam and Eq. 2 is reminiscent of the fundamental period of a two dimensional wedge-shaped beam due to lateral shear vibrations (3,4,7):

$$T_1 \simeq 2.60 \frac{H}{C} \qquad (25b)$$

Therefore, shear deformations are more important than axial deformations in relatively long dams.

Another way of studying the relative significance of axial versus shear deformations is by considering the peak-strain ratio

$$(SR)_{nr} = \frac{\max \epsilon_{x,nr}}{\max \gamma_{zx,nr}} \qquad (26)$$

From Eqs. 18 and 19:

$$(SR)_1 \simeq 3.10 \frac{H}{L} \qquad (26a)$$

which also demonstrates that as the canyon becomes wider (H/L decreases) the importance of shear deformations increases.

Notice also in Fig. 2(*a*) and in Eqs. 24 that Poisson's ratio, ν, has a practically negligible effect on the fundamental frequency. Also negligible is the influence of ν on the higher frequencies. Only results for a typical value of $\nu = 0.40$ are thus shown hereafter, except when otherwise stated.

Fig. 2(*b*) portrays the variation with L/H of the ratio ω_{nr}/ω_{11} of six higher frequencies (n, $r = 1, 2, 3, 4$) over the fundamental frequency. Two conclusions can be drawn: (1) Successive natural frequencies are very close to each other, e.g., a dam with $L/H = 2$ has $\omega_{12} \simeq \omega_{21} \simeq 1.60\ \omega_{11}$, $\omega_{13} \simeq 1.40\ \omega_{12}$, $\omega_{31} \simeq 1.06\ \omega_{13}$, etc., therefore, in general, no reliable estimate of response parameters can be obtained through empirical combination(s) of the maximum modal responses that are determined from a design spectrum (8). Instead, superposition of time histories of modal responses (as Eq. 21) must be performed; and (2)

the ratio ω_{nr}/ω_1 is an increasing or decreasing function of L/H depending on whether n is larger or smaller than r. When $n = r$, the ratio [not shown in Fig. 2(*b*)] has an approximately constant value, i.e., independent of L/H (e.g., $\omega_{22}/\omega_{11} \simeq 2.15$, $\omega_{13}/\omega_{11} \simeq 3.30$, etc.).

Finally, Fig. 3 shows in perspective the deformation of an earth dam in the

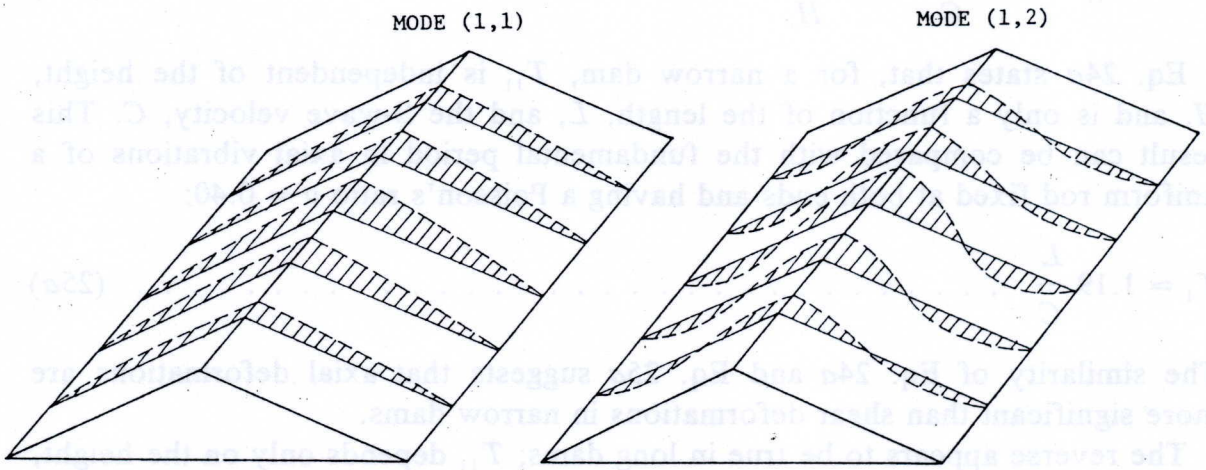

FIG. 3.—Distortion of Dam Vibrating in Two Natural Modes (perspective)

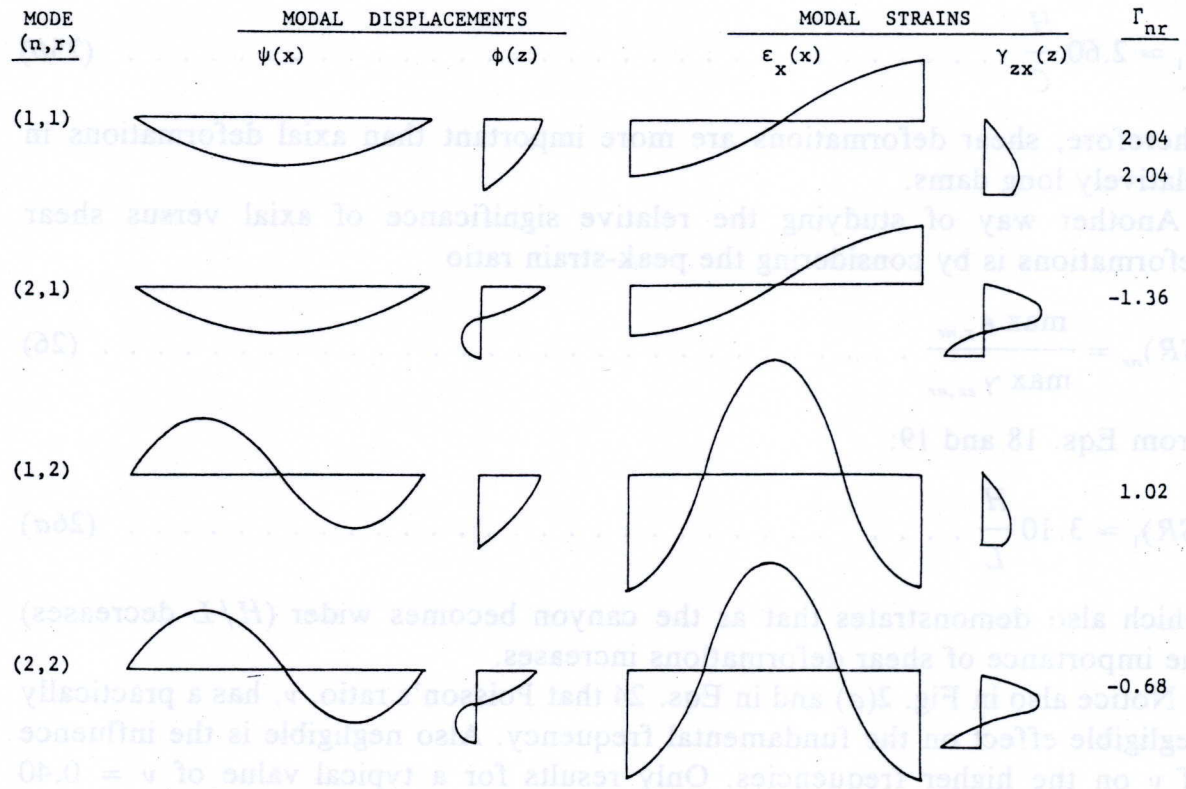

FIG. 4.—Modal Displacement and Modal Strain Components of First Two Symmetric and First Two Antisymmetric Modes

first two symmetrical modes of longitudinal vibrations [(1,1) and (2,1)] and Fig. 4 displays the x and z components of modal displacement shapes with the corresponding axial and shear components of modal strain shapes and the mode participation factors. It can be seen that maximum axial strains (which are of major concern with longitudinal vibrations) develop at the crest level of the abutment dam interface. Significant contributions to these strains come

from both symmetric ($r = 1$) and antisymmetric ($r = 2$) modes of vibration. Maximum shear strains develop at points with $x = L/2$ (middle section) and depth $z \simeq 0.75\ H$ or $0.34\ H$ etc. depending on the mode of vibration ($n = 1$ or 2 etc.).

Case Study I: Santa Felicia Earth Dam

Abdel-Ghaffar and Scott (1) have reported the analyses of two "complete" records of the response of Santa Felicia Dam in Southern California during

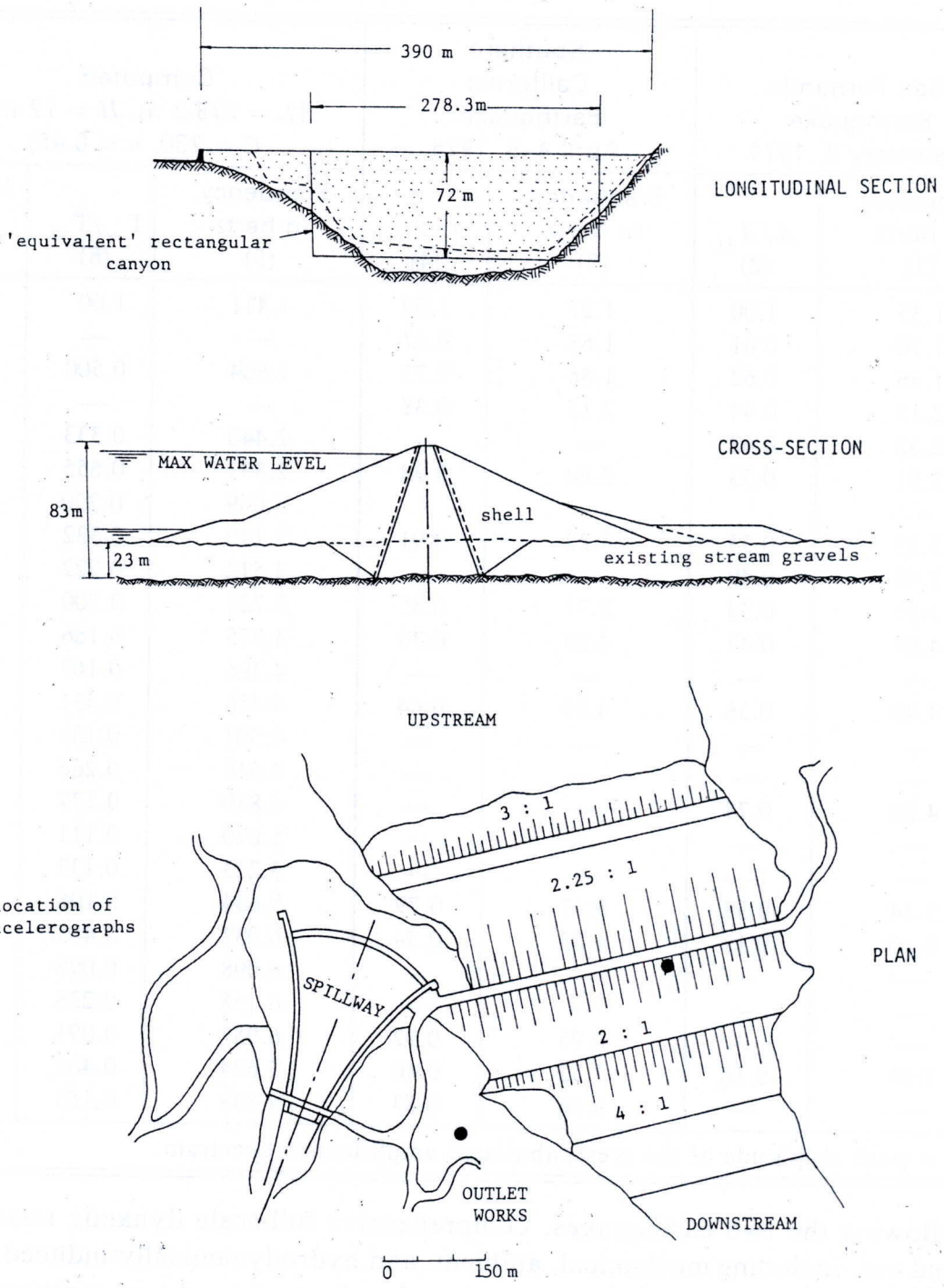

FIG. 5.—Santa Felicia Dam (1)

the San Fernando Earthquake of February 9, 1971 ($M = 6.5$, $R = 33$ km) and the Southern California Earthquake of April 8, 1976 ($M = 5$, $R = 14$

km). Santa Felicia Dam is a modern rolled-fill embankment whose geometric characteristics are shown in Fig. 5 (reproduced from Ref. 1). The dam, located 65 km northwest of Los Angeles, is approx 83 m high above its lowest foundation, 61 m above the original stream bed, and 390 m long at the crest. It has a central impervious core and pervious shells upstream and downstream. All materials are of alluvial origin.

TABLE 1.—Comparison between Computed and Observed Natural Frequencies and Participations: Santa Felicia Dam, California

San Fernando Earthquake: February 9, 1971		Southern California Earthquake: April 4–8, 1976		Computed (L = 278.3 m, H = 72 m, C = 230, ν = 0.45)		
Frequency, in hertz (1)	A/A_{11} (2)	Frequency, in hertz (3)	A/A_{11} (4)	Frequency, in hertz (5)	Γ_{nr}/Γ_{11} (6)	Mode n, r (7)
1.35	1.00	1.27	1.00	1.411	1.00	1, 1
1.70	0.61	1.66	0.67	—	—	—
1.86	0.62	1.86	0.73	1.864	0.500	1, 2
2.15	0.44	2.15	0.38	—	—	—
2.32	0.62	—	—	2.440	0.333	1, 3
2.91	0.53	2.64	0.38	2.893	0.655	2, 1
—		—		3.069	0.250	1, 4
3.15	0.53	3.22	0.91	3.140	0.332	2, 2
3.49	0.49	—	—	3.512	0.222	2, 3
3.85	0.34	3.71	0.55	3.725	0.200	1, 5
4.03	0.43	4.20	0.79	3.975	0.166	2, 4
—	—	—	—	4.396	0.167	1, 6
4.42	0.36	4.59	0.44	4.456	0.531	3, 1
—	—	—	—	4.501	0.133	2, 5
—	—	—	—	4.619	0.266	3, 2
4.88	0.75	—	—	4.880	0.177	3, 3
—	—	—	—	5.070	0.111	2, 6
—	—	—	—	5.223	0.133	3, 4
5.44	0.39	5.57	0.79	5.634	0.106	3, 5
6.10	0.17	6.05	0.54	6.037	0.455	4, 1
—	—	—	—	6.098	0.098	3, 6
—	—	—	—	6.158	0.228	4, 2
—	—	6.93	0.92	6.952	0.091	4, 5
7.91	0.18	7.52	0.40	7.624	0.405	5, 1
—	—	9.96	0.83	9.838	0.153	6, 5

[a] A = peak amplitude of the crest/abutment amplification spectrum.

Following the two earthquakes, comprehensive full-scale dynamic tests were carried out, including mechanical, ambient, and hydrodynamically-induced vibrations (2). Moreover, geophysical tests were performed to obtain representative low-strain values of key soil parameters such as shear-wave velocity (or shear modulus) and Poisson's ratio (1). Wave velocity estimates were also obtained from observed resonant frequencies of lateral vibrations, utilizing existing shear-beam theories (3,7). It was suggested that the average velocity of the

Santa Felicia dam lies between approx 220 m/sec and 270 m/sec, while a Poisson's ratio equal to 0.45 seems reasonable.

An "equivalent" dam in a rectangular canyon shown in Fig. 1(*a*) is chosen to approximate the actual dam geometry. Its dimensions are: $L = 278.3$ m and $H = 72$ m. Shear-wave velocity is taken equal to 230 m/s, i.e., near the lower bound of the suggested range, as is appropriate for relatively strong earthquake motions that are analyzed here.

The ratios of Fourier Spectra, i.e., Amplification Spectra, computed from the two pairs of parallel-to-the-dam-axis components of motions that were recorded at the middle of the crest and the right abutment during the two earthquakes, provide useful information regarding the natural frequencies of the dam in longitudinal vibrations. They also offer a qualitative picture of the degree to which various natural modes participate in the shaking. Table 1 summarizes this information (obtained from Ref. 1) in the form of natural frequencies, f, and ratios of peak amplitudes, A/A_{11}. Also shown in this table are the natural frequencies and mode participation factors computed with the theory presented herein (Eq. 16 and Eq. 22) using the aforementioned values for the material properties and geometry of the dam.

The agreement between predicted and observed natural frequencies is for all purposes satisfactory although some of the predicted higher frequencies are not observed in the recorded motions. Notice, however, the relatively small participation factors of these frequencies.

Direct comparison between ratios of peak amplitudes (A_{nr}/A_{11}) of an amplification spectrum and ratios of participation factors (Γ_{nr}/Γ_{11}) cannot be made Because as it can be seen from Eq. 21

$$\frac{A_{nr}}{A_{11}} = \frac{\Gamma_{nr}}{\Gamma_{11}} \frac{D_{nr}(t)|_{\max}}{D_{11}(t)|_{\max}} \qquad (27)$$

and, unless $D_{nr}(t)\,|_{\max} = D_{11}(t)\,|_{\max}$, the aforementioned two ratios will be different. Nevertheless, one can qualitatively state that the relatively large participation factors predicted by this theory for some of the higher modes of vibration are in accord with the large peak amplitudes of the amplification spectra at the corresponding frequencies.

In conclusion, the presented simple theory of longitudinal vibrations of homogeneous earth dams in rectangular canyons explains with reasonable accuracy the observed behavior (natural frequencies, participation factors) of the Santa Felicia Dam during two Californian earthquakes.

Case Study II: Kisenyama Rockfill Dam

Okamoto (9) reports the motions recorded during a 1969 Earthquake by a number of seismometers that had been installed at the crest, slope, interior, and abutments of the Kisenyama rockfill dam, in Japan. The dam is 95 m high, 255 m long at the crest, and is founded on rock. Fig. 6(*a*) shows a longitudinal and vertical cross section of the dam, while Fig. 6(*b*) shows the parallel-to-the-dam-axis motions recorded at the ground (point 1), at the center of the crest (point 2), and at 25 m below the crest in the clay-core (point 3). The earthquakes occured at the northwestern part of the Giru Prefecture on September 9, 1969, shortly after construction of the dam had been completed. Visual examination

of the records reveals that essentially only the fundamental and a few higher modes of the dam are excited; the motions (at point 2 and point 3) are very nearly sinusoidal with an average period $T = 0.42$ sec. Also apparent is the huge amplification of the motion at the crest (point 2), whereas at a relatively shallow depth of approximately $(1/3)$ H from the crest (point 3), the motion is only moderately higher than the ground motion (point 1). The distribution with depth from the crest of the peak recorded accelerations is depicted in Fig. 6(*c*) (black points).

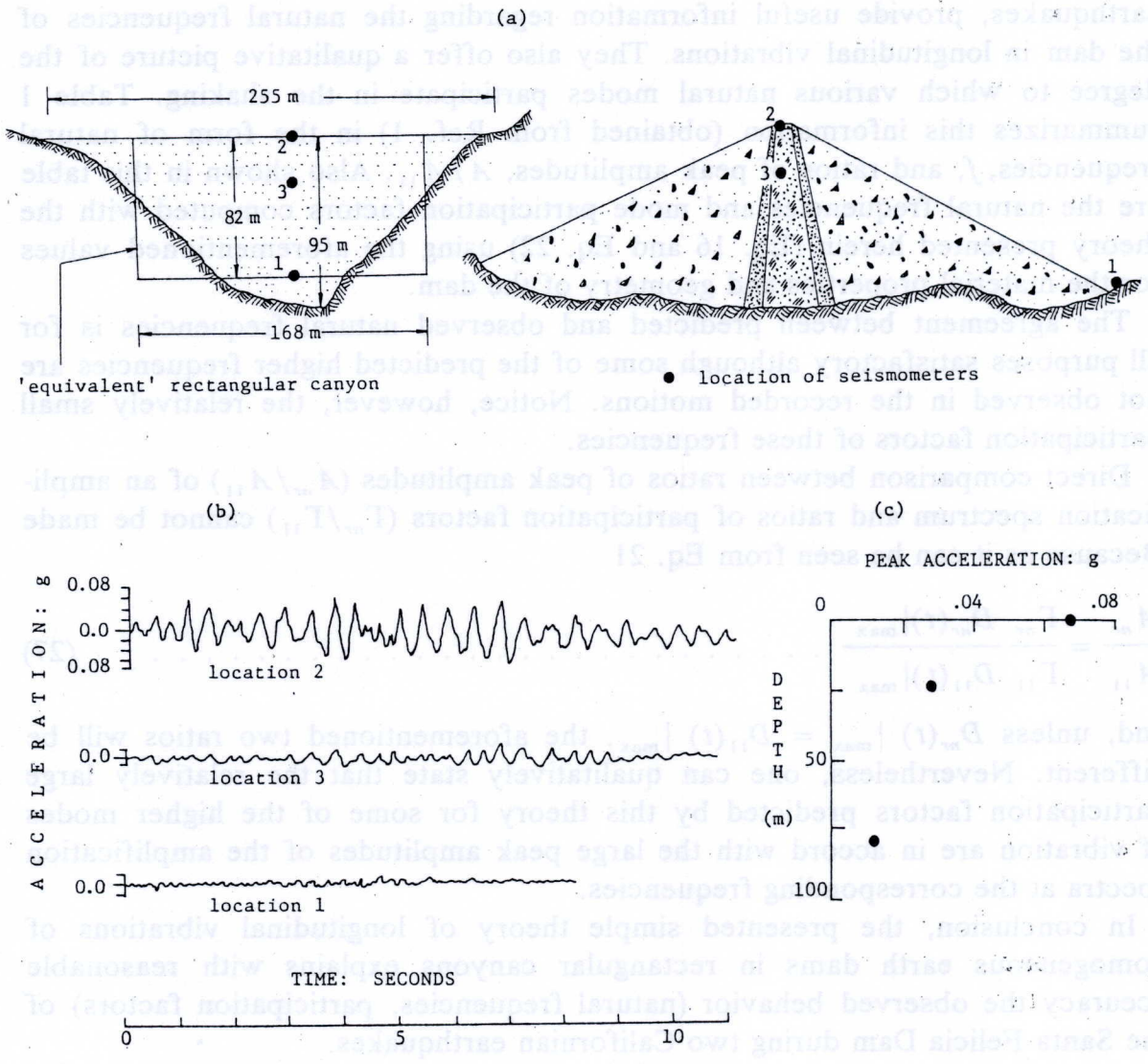

FIG. 6.—Kisenyama Rockfill Dam: (*a*) Geometry; (*b*) Accelerograms in Dam and on Ground; and (*c*) Variation of Peak Acceleration with Depth from Crest

Similar trends are observed in the normal-to-the-dam-axis records (shown in Ref. 9): (1) Nearly sinusoidal motions with an average period $T \simeq 0.48$ sec; and (2) large amplification of the motion near the crest.

Estimation of S-Wave Velocity.—On the basis of the observed fundamental period $T = 0.42$ sec, the theory of longitudinal vibrations of embankment dams presented in this paper can establish an "effective" value of the average S-wave velocity, consistent with the experienced level of shear deformations during this particular earthquake. This velocity can then be utilized to explain the actual response of the dam.

An "equivalent" dam in a rectangular canyon is chosen to approximate the actual geometry, as sketched in Fig. 6(*a*). Its dimensions are $L \simeq 168$ m and $H \simeq 82$ m. Poisson's ratio is taken as $\nu \simeq 0.25$. This is believed to be a representative value for rockfill dams immediately after construction, i.e., before the water of the lake has saturated the clay core.

Now, substituting $T_{11} = 0.42$ sec and the aforementioned geometric and material properties in the frequency relation (Eq. 16) gives:

$$C = \frac{2\pi H}{T_{11}} \left[S_1^2 + 2(1+\nu)\pi^2 \left(\frac{H}{L}\right)^2 \right]^{-1/2}$$

$$\simeq \frac{2\pi(82)}{(0.42)} \left[(2.405)^2 + 2(1.25)\pi^2 \left(\frac{82}{168}\right)^2 \right]^{-1/2} \quad \ldots\ldots\ldots\ldots\ldots\ldots \quad (28)$$

or $C = 359$ m/sec. The theory of lateral shear vibrations of embankment dams in a rectangular canyon (3,7) is subsequently used in connection with the observed fundamental period $T \simeq 0.48$ sec to check the accuracy of the preceding value of velocity. Solving for C, the corresponding frequency equation, e.g., Eq. 12 in Ref. 3, one obtains:

$$C = \frac{2\pi H}{T_{11}} \left[S_1^2 + \pi^2 \left(\frac{H}{L}\right)^2 \right]^{-1/2} \simeq \frac{2\pi(82)}{0.48} \left[(2.405)^2 + \pi^2 \left(\frac{82}{168}\right)^2 \right]^{-1/2} \quad (29)$$

or $C = 375$ m/sec. The two backfigured values of C are in fairly good agreement with each other (difference ≃4%). Moreover, 359 m/sec–375 m/sec is a realistic range for the S-wave velocity of a rockfill dam experiencing moderate levels of excitation (≃0.10 g peak-crest acceleration in the lateral direction; and ≃0.07 g in the longitudinal direction).

The natural periods of the two higher symmetric modes of vibrations are obtained by means of Fig. 2(*b*) (or through Eq. 16):

$$T_{21} \simeq \frac{T_{11}}{1.68} \simeq 0.25 \text{ sec} \quad \ldots\ldots\ldots\ldots\ldots\ldots\ldots\ldots\ldots\ldots \quad (30a)$$

$$T_{31} \simeq \frac{T_{11}}{2.58} \simeq 0.16 \text{ sec} \quad \ldots\ldots\ldots\ldots\ldots\ldots\ldots\ldots\ldots\ldots \quad (30b)$$

One can easily identify these two modes with some of the peaks of the recorded motions, e.g., the crest accelerogram (point 2) at time $t \simeq 2$ sec and in the time interval between 4 sec and 5 sec consists of cycles having periods around 0.20 sec. Note, also, that the higher antisymmetric modes [(1,2), (1,3), etc.] have a negligible contribution to the motion of points 2 and 3 because they are located close to the central cross section of the dam, i.e., at $x = L/2$.

Distribution of Peak Responses along Height of Dam.—To explain the sharp increase of the motion near the crest of the dam in comparison with the motion at a depth of only 25 m (≃0.305 H) from the crest, one can use the presented theory to compute the acceleration ratio

$$AR = \frac{\max \ddot{u}_2(t)}{\max \ddot{u}_3(t)} \quad \ldots\ldots\ldots\ldots\ldots\ldots\ldots\ldots\ldots\ldots \quad (31)$$

The acceleration time histories at points 2 and 3, $\ddot{u}_2(t)$ and $\ddot{u}_3(t)$, can be numerically obtained by means of Eq. 21 after evaluation of the Duhamel integral (Eq. 23). Unfortunately, however, the ground record $\ddot{u}_{gx}(t)$ is not available in digitized form and in order to roughly estimate AR the response spectrum approach (8) is used with the following two simplifying assumptions: (1) Only the first three symmetric natural modes ($n = 1, 2, 3$; $r = 1$) participate in the motion; and (2) the spectral accelerations, S_a, that correspond to each of the three first natural periods are all equal. The first assumption is by no means arbitrary, as it is evident from the appearance of the two accelerograms and the previous

TABLE 2.—Predictions of Peak Acceleration Distribution in Kisenyama Rockfill Dam in Japan (9)

Rule of Combining Modal Maxima		ASSUMPTION: $S_a(T_{11}) = S_a(T_{21}) = S_a(T_{31}) \equiv S_a$					
		'HOMOGENEOUS' THEORY			'INHOMOGENEOUS' THEORY		
No	Expression	$\frac{\max \ddot{u}_2}{S_a}$	$\frac{\max \ddot{u}_3}{S_a}$	AR	$\frac{\max \ddot{u}_2}{S_a}$	$\frac{\max \ddot{u}_3}{S_a}$	AR
1	$\sqrt{\sum_{i=1}^{3} Q_i^2}$	2.67	1.86	1.43	3.46	1.46	2.37
2*	$\sqrt{\sum_{i=1}^{3} Q_i^2 + \sum\sum_{i=j} \frac{Q_i Q_j}{1+\varepsilon_{ij}^2}}$	2.61	1.82	1.44	3.36	1.43	2.33
3	$Q_1 + \frac{1}{2}\sqrt{\sum_{i=2}^{3} Q_i^2}$	2.90	2.06	1.40	3.41	1.62	2.10
		ASSUMPTION: $S_a(T_{21}) = S_a(T_{31}) = 2 \cdot S_a(T_{11}) \equiv 2 \cdot S_a$					
1	$\sqrt{\sum_{i=1}^{3} Q_i^2}$	3.99	2.11	1.88	6	1.67	3.57

OBSERVED RATIO: AR ≈ 2.34

* $\varepsilon_{ij} \simeq \frac{\omega_i' - \omega_j'}{\beta_j' \omega_i + \beta_j' \omega_j}$, $\beta_i' = \beta_i + \frac{2}{\omega_i t}$, $\omega_i' = \omega_i [1-\beta_i^2]^{1/2}$ [Ref. 7]

analysis regarding the natural periods of the dam. However, since the details of the response spectrum are unknown, the second assumption can only be considered as a crude, although reasonable, simplification. Its justification stems from the observation (8,9) that usually damped acceleration spectra exhibit a more or less constant value in the period range between 0.16 sec and 0.42 sec, i.e., in the range of the three natural periods of interest. This would especially be so for the large value of critical damping ratio (of the order of 5%–10%) that most probably developed in the soil during this particular earthquake.

For each of the two points (2 and 3) the maximum acceleration due to each

of the three symmetric modes is obtained from

$$Q_n = \max \ddot{u}_{n1} = \Gamma_{n1} U_{n1} S_a; \quad n = 1, 2, 3 \quad \ldots\ldots\ldots\ldots\ldots\ldots\ldots\ldots (32)$$

in which the participation factors, Γ_{n1}, and modal shapes, U_{n1}, of the $(n, 1)$ mode are obtained from Eqs. 22 and 17, respectively. The individual modal maxima are then combined by three empirical rules to provide an estimate of the overall expected peak accelerations. Table 2 displays the results and explains the expressions of the three rules. The "square root of the sum of the squares" (SRSS) is the most popular of these rules (8,9) but it probably overestimates the total-peak response in this case because of the proximity of the natural frequencies of the dam (a phenomenon already addressed in a previous section). The second rule, suggested by Rosenblueth (8), is perhaps more appropriate since it accounts for the interaction between modal contributions. Finally, the third rule attempts to reflect the greater importance of the fundamental mode, as seen in the two records.

The results of Table 2 demonstrate that the simple theory of longitudinal vibrations, as presented so far, cannot adequately explain the observed high amplification of the seismic motion near the crest. All three rules yield quite similar acceleration ratios not exceeding 1.44, which is only 60% of the ratio of recorded peak accelerations: $0.68/0.29 \simeq 2.34$. Of course, one might argue that higher spectral accelerations at the second and third periods (0.25 sec and 0.16 sec) would have favored the corresponding higher modes and, thus, led to prediction of sharper near-crest amplification. Nevertheless, even if one assumes $S_a(T_{21}) = S_a(T_{31}) = 2 \cdot S_a(T_{11})$, the resulting acceleration ratio will not exceed the value of 1.88 (shown also in Table 2). Larger differences in the spectral accelerations (than the factor 2 implies) are highly improbable given the relatively large amount of damping the dam must have experienced during the earthquake. After all, the two records bear no evidence whatsoever of any predominance of the higher modes. Note, furthermore, that lateral vibrations exhibited a similarly sharp amplification near the crest (8), as mentioned previously, although the corresponding natural periods (0.48 sec, 0.235 sec, and 0.158 sec) differ somewhat from the periods of longitudinal vibrations.

In conclusion, the simple theory that was previously presented cannot explain the distribution of peak responses along the height of the dam. It is believed the soil inhomogeneity, which the theory does not account for, is the primary factor that causes its failure.

Simple Model that Accounts for Soil Inhomogeneity

Shear modulus even within a uniform mass of soil is not constant but increases approximately as the square-root of the effective normal octahedral stress: $G \sim (\sigma_0')^{1/2}$. Plane-strain finite-element analyses of the static stress distribution in typical dam cross sections (Ref. 5) suggest in a reasonably consistent way that, with good accuracy, the average σ_0' across the dam width is an increasing function of the distance from the crest:

$$\sigma_0' \sim z^{4/3} \quad \ldots\ldots\ldots\ldots\ldots\ldots\ldots\ldots\ldots\ldots\ldots\ldots\ldots\ldots (34)$$

Thus, it appears that the average shear modulus across the width of a dam increases as the two-third power of the depth z. The result of geophysical

investigations on numerous earth and rockfill dams in the United States and Japan have confirmed this form of variation of soil stiffness in embankment-type dams (5,6). The writer (4,5) has recently presented a theory of lateral shear vibrations of earth dams whose modulus varies in proportion to $z^{2/3}$. Successful evaluation of this theory in the light of recorded responses of several dams from United States, Japan, and Yugoslavia during earthquake, forced, and ambient vibrations (5,6), offers additional indirect evidence of the appropriateness of Eq. 34.

It is concluded that embankment dams are inhomogeneous in the vertical direction. It would, therefore, be necessary to modify the presented theory of longitudinal vibrations in order to account for an S-wave velocity that increases with depth according to:

$$\frac{C}{C_m} = \left(\frac{z}{H}\right)^{1/3} \quad (34)$$

in which C_m = the velocity at the base of the dam, i.e., at $z = H$.

Exact analytical solution of the governing differential equation of free vibrations (Eq. 1) is impossible if the soil properties are described by Eq. 34 and by a constant Poisson's ratio. A simple approximate solution can, however, be obtained by heuristically combining the solution of two extreme cases: (1) The case of a "very" long dam; and (2) the case of a "very" narrow dam. As explained previously (Eqs. 24 and 26), shear deformations are predominant in case 1, whereas axial deformations are predominant in case 2. Accordingly, in the first case, Eq. 1 is simplified to

$$-\rho\omega^2\Phi \simeq \frac{1}{z}\frac{d}{dz}\left(Gz\frac{d\Phi}{dz}\right);$$

$$\text{with} \quad G = G(z) = \rho\, C^2 = \rho\, C_m^2 \left(\frac{z}{H}\right)^{2/3} \quad (35)$$

and in the second case to

$$-\rho\omega^2\Psi \simeq 2(1+\nu)\,\bar{G}\,\frac{d^2\Psi}{dx^2} \quad (36)$$

with $\bar{G} = (6/7)^2\,\rho\,C_m^2$ being the average shear modulus.

The exact solution of Eq. 35 that satisfies the boundary conditions (Eq. 4 and Eq. 5) is

$$\Phi_n(z) = \frac{1}{z^{2/3}}\sin\left\{n\pi\left[1-\left(\frac{z}{H}\right)^{2/3}\right]\right\}; \quad n = 1, 2, 3, \ldots \quad (37)$$

and the corresponding eigenvalues are

$$\omega_n = \frac{7\pi}{9}\frac{\bar{C}}{H}n; \quad n = 1, 2, 3, \ldots \quad (38)$$

in which $\bar{C} = (6/7)\,C_m$ is the average S-wave velocity. The reader is referred to Ref. 4 for a detailed derivation of this solution. Direct substitution of Eq. 37 and Eq. 38 in Eq. 35 is, however, sufficient to convince of its correctness.

The solution of Eq. 36 and the corresponding and eigenvalues are

$$\Psi_r(x) = \sin\left(r\pi\frac{x}{L}\right) \quad \ldots\ldots\ldots\ldots\ldots\ldots\ldots\ldots\ldots\ldots\ldots\ldots \quad (39)$$

$$\omega_r = \pi\,[2(1+\nu)]^{1/2}\frac{\bar{C}}{L}r; \quad r = 1, 2, 3, \ldots \quad \ldots\ldots\ldots\ldots\ldots\ldots\ldots\ldots \quad (40)$$

In heuristic fashion, guided by the form of Eqs. 16 and 17, one can combine Eqs. 37–39 and Eqs. 38–40 to obtain approximate general formulas for the longitudinal mode shapes and natural frequencies of an embankment dam whose moduli increase with the 2/3 power of depth:

$$U_{nr} \simeq \frac{1}{z^{2/3}}\sin\left\{n\pi\left[1-\left(\frac{z}{H}\right)^{2/3}\right]\right\}\sin\left(\frac{r\pi x}{L}\right) \quad \ldots\ldots\ldots\ldots\ldots\ldots\ldots \quad (41)$$

$$\omega_{nr} \simeq \frac{\bar{C}}{H}\left[\left(\frac{7\pi}{9}n\right)^2 + 2(1+\nu)\pi^2\left(\frac{H}{L}\right)^2 r^2\right]^{1/2}; \quad n, r = 1, 2, 3, \ldots\ldots \quad (42)$$

The modal participation factor due to earthquake shaking that consists of vertically propagating waves is also given here:

$$\Gamma_{nr} = \frac{8}{\pi^2 nr} \quad \ldots\ldots\ldots\ldots\ldots\ldots\ldots\ldots\ldots\ldots\ldots\ldots\ldots\ldots \quad (43)$$

Notice that despite its approximate character, the preceding solution is exact in the two limiting cases of $L/H \to 0$ (narrow dam) and of $L/H \to \infty$ (long dam). It is moreover believed that for intermediate ranges of the L/H ratio, Eqs. 41 and 42 describe the behavior of the dam more accurately than Eqs. 16 and 17, since the former capture both the two dimensional character of the response and the inhomogeneous nature of the material properties.

Comparison of Eq. 42 and Eq. 16, portrayed in Fig. 7(*a*), reveals that the two theories (hereafter referred to as "homogeneous" or "inhomogeneous") predict very similar natural frequencies. The maximum discrepancy between fundamental frequencies is only 1.6%, in the extreme case of $L/H = \infty$; it tends to zero as L/H decreases. Larger discrepancies are observed with the higher modes, as the inhomogeneous theory predicts frequencies that are closer to the fundamental frequency, in comparison with the higher frequencies of the homogeneous theory (Eq. 16), e.g., for a very long dam Eq. 42 yields

$$\frac{\omega_{21}}{\omega_{11}} \simeq 2 \quad \text{and} \quad \frac{\omega_{31}}{\omega_{11}} \simeq 3 \quad \ldots\ldots\ldots\ldots\ldots\ldots\ldots\ldots\ldots\ldots\ldots\ldots \quad (44a)$$

whereas Eq. 16 gives

$$\frac{\omega_{21}}{\omega_{11}} \simeq 2.3 \quad \text{and} \quad \frac{\omega_{31}}{\omega_{11}} \simeq 3.6 \quad \ldots\ldots\ldots\ldots\ldots\ldots\ldots\ldots\ldots\ldots\ldots\ldots \quad (44b)$$

As, however, L/H decreases, the discrepancies become insignificant converging to zero for $L/H \to 0$ [Fig. 7(*a*)].

The important difference between the two theories lies in their mode shapes. As shown in Fig. 7(*b*), the inhomogeneous theory (Eq. 41) leads to a sharp

deamplification of modal displacements with depth, not anticipated by the homogeneous theory (Eq. 16). This discrepancy is not decreasing with L/H, although its consequence on the shear-strain/axial-strain ratio is, indeed, diminishing as the dam becomes narrower.

Reinterpretation of Kisenyama Dam Records.—The new theory appears to be able to explain the sharp increase of motion near the crest of the Kisenyama rockfill dam during the September 9, 1969 earthquake.

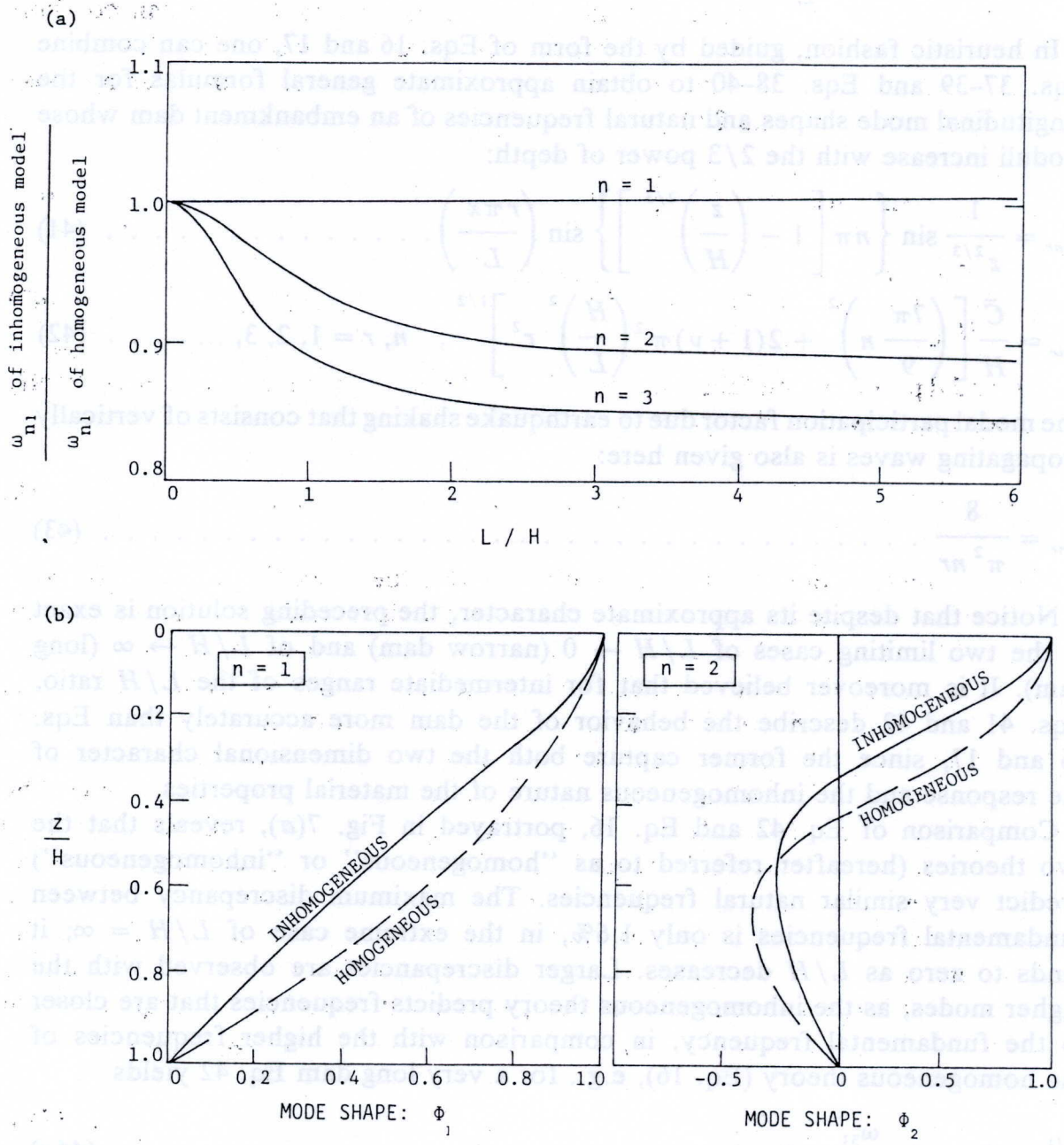

FIG. 7.—Comparison of: (*a*) Three Natural Frequencies; and (*b*) Vertical Components of Two Mode Shapes Obtained with Homogeneous (Eqs. 16, 17) and Inhomogeneous Models (Eqs. 41, 42)

First, using Eq. 42 instead of Eq. 16, the effective S-wave velocity of the dam during this earthquake is estimated to be

$$\bar{C} \simeq \frac{2\pi(82)}{(0.42)}\left[(2.443)^2 + 2(1.25)\pi^2\left(\frac{82}{168}\right)^2\right]^{-1/2} \simeq 356\,\frac{\text{m}}{\text{s}} \quad \ldots\ldots\ldots \quad (45)$$

i.e., smaller by only about 0.84% than the value 359 m/s derived previously from Eq. 16.

The natural periods of the two higher symmetric modes are now expected to be [Fig. 6(*a*)]

$$T_{21} \simeq \frac{T_{11}}{1.58} \simeq 0.27 \text{ sec} \quad \ldots\ldots\ldots\ldots\ldots\ldots\ldots\ldots\ldots\ldots \quad (46a)$$

$$T_{31} \simeq \frac{T_{11}}{2.24} \simeq 0.19 \text{ sec} \quad \ldots\ldots\ldots\ldots\ldots\ldots\ldots\ldots\ldots\ldots \quad (46b)$$

compared with the values of 0.25 sec and 0.16 sec derived from Fig. 2(*b*).

Finally, the peak accelerations at points 2 and 3 are reestimated on the basis of the same, aforementioned assumptions, i.e., only three modes participate in the motion; the corresponding three spectral accelerations are the same. The results are displayed in Table 2 for all three rules of combining modal maxima. The agreement of the predicted peak acceleration ratios with the observed value of 2.34 clearly demonstrates that inhomogeneity (of the form described by Eqs. 33 or 34) has been the primary factor that caused the high amplification of the motion near the top of the dam. Also shown in this table is the prediction of the peak values and their ratio under the assumption that the spectral acceleration, S_a, of the second and third higher modes is two times larger than the spectral acceleration of the fundamental mode. The result ($AR \simeq 3.57 > 2.34$) further supports the assumption of not very different S_a values for the three modes. Thus, it appears that the homogeneous theory cannot even roughly explain the observed distribution of accelerations along the height of the dam. The superiority of the inhomogeneous theory, in this respect, is clear. Whether or not the theory will always yield results comparing as favorably with reality as in this single case, remains to be seen. The reader is cautioned, nevertheless, that factors other than those accounted for by the theory, such as the nonrectangular geometry of the canyon and the nonlinear soil deformations during strong, earthquake-induced vibrations, may also play a predominant role in certain cases. Their effect should, therefore, at least qualitatively be assessed when studying the longitudinal as well as the lateral vibrational behavior of earth and rockfill dams.

Summary and Conclusions

Longitudinal vibrations of embankment dams are of concern in geotechnical engineering since they can cause transverse cracking at the abutment dam or the dam-outlet works interfaces. Such cracking is quite dangerous as it may allow water to flow through the dam and thus lead to piping failure.

Free and forced longitudinal vibrations of embankment dams in a rectangular canyon have been studied with a method that accounts for both shear and dilatational deformations and models the dam as a linear homogeneous medium. Presented numerical results demonstrate the effect of the length and height of the dam on its natural frequencies and its modal displacement and strain shapes. The method has been successfully evaluated by comparing the predicted natural frequencies for the Santa Felicia Dam with the observed predominant

frequencies of the amplification spectra obtained from recorded motions on this Dam during two earthquakes (1).

Failure of the method to explain the observed sharp increase of the motion near the crest of the Kiseneyama rockfill dam in Japan during a moderate earthquake (9) motivated the study of the importance of soil inhomogeneity. An approximate method has thus been developed that considers the shear modulus in the dam as increasing with the 2/3 power of depth, a variation that has been confirmed from in situ measurement in several dams (1,2,5,6). This simple "inhomogeneous" method is negligibly different from the "homogeneous" theory when natural frequencies are compared. It yields, however, mode shapes that exhibit a sharp attenuation with depth near the crest, and, consequently, it explains very well the observed behavior of the Kisenyama Dam.

In conclusion, it appears that additional theoretical and, even more, experimental research may be needed in order to develop reliable methods of design of embankment dams to resist longitudinal vibrations.

Acknowledgment

The writer acknowledges useful comments by the ASCE reviewers.

Appendix.—References

1. Abdel-Ghaffar, A. M., and Scott, R. F., "An Investigation of the Dynamic Characteristics of an Earth Dam," *Earthquake Engineering Research Laboratory Report EERL 78-02*, California Institute of Technology, Pasadena, Calif., 1978.
2. Abdel-Ghaffar, A. M., Scott, R. F., and Craig, M. J., "Full-Scale Experimental Investigation of a Modern Earth Dam," *Earthquake Engineering Research Laboratory Report EERL 80-02*, California Institute of Technology, Pasadena, Calif., 1978.
3. Ambraseys, N. N., "On the Shear Response of a Two-Dimensional Truncated Wedge Subjected to an Arbitrary Disturbance," *Bulletin of the Seismological Society of America*, Vol. 50, No. 1, 1960, pp. 45–56.
4. Gazetas, G., "Shear Vibrations of Vertically Inhomogeneous Earth Dams," *International Journal for Numerical and Analytical Methods in Geomechanics*, 1981.
5. Gazetas, G., "A New Dynamic Model for Earth Dams Evaluated Through Case Histories," *Soils and Foundations*, Japanese Society of Civil Engineers, 1981.
6. Gazetas, G., and Abdel-Ghaffar, A. M., "Earth Dam Characteristics from Full-Scale Vibrations," to be presented at the June, 1981, International Conference of Soil Mechanics and Foundation Engineering, to be held at Stockholm, Sweden.
7. Hatanaka, M., "Fundamental Considerations on the Earthquake Resistant Properties of the Earth Dam," *Disaster Prevention Research Institute Bulletin No. 41*, Kyoto University, Kyoto, Japan, 1955.
8. Newmark, N. M., and Rosenblueth, E., *Fundamentals of Earthquake Engineering*, Prentice-Hall, Inc., Englewood Cliffs, N.J., 1971.
9. Okamoto, S., *Introduction to Earthquake Engineering*, John Wiley and Sons, Inc., New York, N.Y., 1973.
10. Seed, H. B., and Martin, G. R., "The Seismic Coefficient in Earth Dam Design," *Journal of the Soil Mechanics and Foundations Division*, ASCE, Vol. 92, No. SM3, Proc. Paper 4824, May, 1966, pp. 25–58.
11. Seed, H. B., "Considerations of Earthquake Resistance of Earth and Rockfill Dams," *Geotechnique*, Vol. 29, No. 3, 1979, pp. 15–63.